ISSN 1063-7842, Technical Physics, 2012, Vol. 57, No. 11, pp. 1519–1528. © Pleiades Publishing, Ltd., 2012.
Original Russian Text © V.O. Gladyshev, P.S. Tiunov, A.D. Leont'ev, T.M. Gladysheva, E.A. Sharandin, 2012, published in Zhurnal Tekhnicheskoi Fiziki, 2012, Vol. 82, No. 11, pp. 54–63.

OPTICS, QUANTUM ELECTRONICS

Anisotropy of the Velocity Space of Electromagnetic Radiation in a Moving Medium

V. O. Gladyshev*, P. S. Tiunov, A. D. Leont'ev, T. M. Gladysheva, and E. A. Sharandin

Bauman State Technical University, Vtoraya Baumanskaya ul. 5, Moscow, 105005 Russia
**e-mail: vgladyshev@mail.ru*

Received October 18, 2011

Abstract—Anisotropy arising in moving media is considered. In these media, the phase velocity of light nonlinearly depends on the velocity vector field of the medium due to anisotropic binding forces between lattice atoms. Observations of the optical anisotropy of light in a rotating optically transparent medium are discussed. Laser radiation with wavelength $\lambda = 0.632991 \pm 1 \times 10^{-7}$ μm propagating in an interferometer was passed through a rotating optical disk $D = 62$ mm in diameter. The projection of the beam's path length in the medium onto the flat surface of the disk is $l = 41$ mm; the refractive index of the glass and its thickness are, respectively, $n = 1.71250$ for $\lambda = 632.8$ nm and 10 mm; and the angle of incidence of the beam on the flat surface of the disk is $\vartheta_0 = 60°$. The optical disk is rotated in two directions, and its rotation frequency may reach 250 Hz. Experimental data confirm the linear dependence of the fringe shift on the velocity of the medium up to 29.6 m/s. The measurement accuracy is sufficient to detect angular variations $\delta\Delta = 3 \times 10^{-5}$ in the position of fringes at a fixed rotation velocity of the optical disk.

DOI: 10.1134/S1063784212110114

INTRODUCTION

The optics of moving media goes beyond the classical Sagnac, Fizeau, Doppler, and Fermi effects. In the general case of 3D motion of the medium, the propagation of electromagnetic radiation is theoretically described by solving a dispersion relation for the optics of moving media [1]. Therefore, all characteristics of electromagnetic radiation become dependent on the velocities of the media and interfaces. As a result, the theory predicts the violation of the Snell refraction law, variation of the amplitude and phase of transmitted and reflected waves, distortion of the light wave wavevector trajectory in a medium with a 3D law of motion, and other effects.

However, the solution to the dispersion relation was experimentally verified only in a number of particular cases. The best known examples here are studies of the Doppler effect and interferometric experiments on detecting the Sagnac [2] and Fizeau [3] effects.

In a Sagnac-type interferometer, the shift of an interference pattern is due largely to the shift of mirrors during experiments. Theoretically, the Sagnac effect is usually described in terms of electrodynamics equations in a rotating frame of reference [4]. This is possible, since the medium, radiation source, and detector are in the same frame of reference.

If the velocity of the medium moving relative to a radiation source and a detector does not contain a tangential component ($u_{2l} = 0$, $u_{2n} \neq 0$), the longitudinal entrainment of light arises—the effect discovered in the classical Fizeau experiment [3]. The Fizeau effect is much weaker than the Sagnac effect, since the former is associated with a change in the velocity of light in a moving medium, which is proportional to the Fresnel factor in a first approximation. Note that in the Fizeau experiment, there were neither normal nor tangential discontinuities of the velocity at interfaces, which greatly simplifies the solution to the dispersion relation and correspondingly an expression for the phase incursion. These phenomena can be theoretically described in a co-moving frame of reference, which allows neglect of the Fizeau and Doppler effects [5].

More detailed analysis shows that, if refractive index n of a moving medium in the Sagnac experiment is greater than unity ($n > 1$) and the radiation source and detector are removed from the rotating frame of reference into the inertial one, the trajectory of the wavevector can be expected to curve [6]. If the latter condition is not fulfilled, the interference pattern does not depend on the refractive index in a nonrelativistic approximation, as was theoretically proved in [7, 8].

Remarkably, computational results indicate that an additional phase difference due to the beam curvature is comparable in order of magnitude to the phase difference due to the Fizeau longitudinal effect. This is because the Snell law is violated at a tangential discontinuity of the velocity. This, along with the curvature of the trajectory, is expected to shift the point at which the beam escapes from the medium. This complex phenomenon reflects the transverse entrainment of light in a moving medium.

The transverse entrainment of light may arise when radiation propagates in a rotating optical disk. Such an experiment was carried out by Bilger and Stowell [9], who studied light propagation in a rotating optical disk placed in a ring interferometer. They observed the Fizeau effect but did not discover the Snell law violation at the interface (in a rotating disk, the velocity experiences a tangential discontinuity on the flat surface). Moreover, when theoretically describing the results, Bilger and Stowell ignored an additional deflection of the light beam at the tangential discontinuity of the velocity. However, calculations based on solving the dispersion relation indicate that an additional shift of the interference pattern in such experiments may reach about 30% of the value due to the Fizeau effect.

The coordinate solution to the dispersion relation obtained in [1] was based on the assumption that the refractive indices of moving and quiescent media are the same. However, this assumption is of limited use. Of interest in this respect are experiments [10–12] aimed at measuring the dispersion term in the Fresnel and Lorentz formulas for fiber-optic gyros. The application of a very long low-loss optical light guide in a ring interferometer allowed the researchers to measure the Fizeau effect in a rotating fiber and experimentally confirm the presence of a dispersion term in the drag (entrainment) coefficient.

In [13], experiments were carried out in the presence of the normal component of the interface velocity. The results of those experiments were used to check solutions to the equations of electrodynamics of near-relativistic media.

The results mentioned above suggest that an exact solution to the dispersion relation should be used in description of light propagation in moving media. This solution must have terms of the second order of smallness in ratio of the interface velocity or the velocity of the medium to the velocity of light in vacuum, $\beta^2 = V^2/c^2$. The need for taking into account ratio β^2 to correctly describe the spatial Fizeau effect was also theoretically substantiated in [14]. For example, the degree of distortion of the electromagnetic wave trajectory in a medium with rotation has an order of smallness comparable to the computational error when terms containing β^2 are neglected.

The experimental data mentioned above can be viewed only as tests for certain parts of the electrodynamics equations. These parts may be related either to the motion of interfaces (but not media themselves!) or, conversely, to the motion of media with quiescent interfaces. However, effects inherent in the optics of moving media may influence measuring data. For example, in experiments on space vehicle location, the entrainment of light by the moving medium had a considerable influence on the direction of a laser beam passing through a moving quartz reflector. The description of these experiments, together with attempts to theoretically explain the respective experimental data, is given in [15, 16]. Correct interpretation of these experiments in particular and the spatial effect of electromagnetic wave entrainment by a moving medium in general are only possible by solving the dispersion relation. Accordingly, there arises the need to experimentally check the solution for the most general case of moving media.

The propagation of an electromagnetic wave through a medium with rotation makes it possible to experimentally test those parts of the coordinate solutions of the dispersion relation that contain the tangential, u_{2t}, and normal, u_{2n}, components of the velocity of the medium and are responsible for the spatial effect of light entrainment.

To study the relativistic effect of light entrainment in a moving medium, an interferometer with a nonconfocal resonator filled with a transparent medium was suggested [6]. The resonator is a rotating optical disk, from the cylindrical surface of which beams rereflect. Another implementation of the experiment is to introduce radiation through the flat surface of the rotating optical disk. Such an experiment was carried out in [17], where beams were rereflected from the specular parts of the disk's flat surface to increase the optical path length in the disk. Experimental results confirmed calculation data based on the exact solution to the dispersion relation, which takes into account the Snell law violation. To gain a deeper insight into the propagation of electromagnetic radiation in a rotating medium, the optics of the interferometer was modified and the disk's rotation frequency and the refractive index of the medium for beams passing through the disk in opposite directions were increased [18]. It was shown that the degree of entrainment of light in a rotating medium linearly depends on the rotating frequency in a first approximation. Fringe location error $\delta\Delta$ was about 1.4×10^{-3}.

In addition, the constructed interferometer was suggested to be applied for detection of spatial anisotropy under laboratory conditions [18, 19]. Such experiments require high sensitivity to the fringe shift at a low noise level.

A further increase in the signal-to-noise ratio necessitated a number of changes aimed at increasing parameter $\kappa_2 l V_{2n}$ responsible for the light entrainment efficiency in a moving medium, suppressing vibrations, calibrating the interferometer, and automating the experiment. In this work, we report experimental data corroborating the linear dependence of the Fizeau effect on the velocity of the medium at a new level of accuracy.

LONGITUDINAL AND TRANSVERSE ENTRAINMENT OF LIGHT IN A MOVING MEDIUM

A phase difference between two interfering beams having passed through an optical medium in opposite directions depends on the transverse and longitudinal

effects of electromagnetic wave entrainment. Under certain conditions, the transverse entrainment may be comparable to the longitudinal entrainment. Below, we consider the combined influence of the transverse and longitudinal entrainments of a plane monochromatic electromagnetic wave in an optically transparent rotating medium in terms of geometrical optics and find the values of parameters that provide the maximal transverse entrainment. Note that the transverse entrainment of a light beam in a rotating medium is a particular case of distortion of the electromagnetic wave vector trajectory [6].

Let an electromagnetic wave with wavevector $\mathbf{k}_0$ be incident on the flat surface of an optical disk at angle ϑ_0 in the *YAP* plane (Fig. 1). The disk has radius R_0 and rotates with angular velocity ω.

The top and bottom surfaces of the optical disk have reflection coatings with radius R_1. Since the Snell law is violated, refraction angle ϑ_2 becomes equal to angle $\tilde{\vartheta}^2$ for the given direction and point B of the beam escape shifts to point B'. The distance between the beam's projection (the AP axis) and the center of the disk is $r = R\sin\vartheta$, where $R = OA$ is the distance from the point of incidence of the beam to the center of the disk.

Consider the propagation of a plane monochromatic electromagnetic wave in a rotating optical disk in terms of geometrical optics. Let a light beam be divided into two beams by a semitransparent beam splitter, which pass through the rotating optical disk in opposite directions. In the general case, the optical path difference of the beams having passed through the disk in opposite directions can be expressed in units of wavelength as

$$\Delta = \frac{1}{2\pi}\left\{\int_0^\tau(\omega_2(t)-\omega_1(t))dt + \frac{1}{c}\left[\int_0^{S_1}\omega_1(S)n_1(S)dS - \int_0^{S_2}\omega_2(S)n_2(S)dS\right]\right\}. \quad (1)$$

Here, τ is the instant of interference pattern observation; c is the velocity of light in vacuum; and ω_i, S_i, and n_i are, respectively, the circular frequency, geometrical path, and refractive index of the medium for the ith beam ($i = 1, 2$). The frequency of the electromagnetic wave traveling in the interferometer becomes time-dependent when moving optical elements interacting with the wave have normal components of the velocity. However, if the interferometer moves with a constant velocity as a whole, one can always select an inertial frame of reference in which the normal components of the velocities of interfaces equal zero for all the elements, $\omega_1 = \omega_2$, and the first integral in expression (1) vanishes. In this case, the two remaining integrals simplify considerably and, if the refractive indices are constant, expression (1) takes a trivial form.

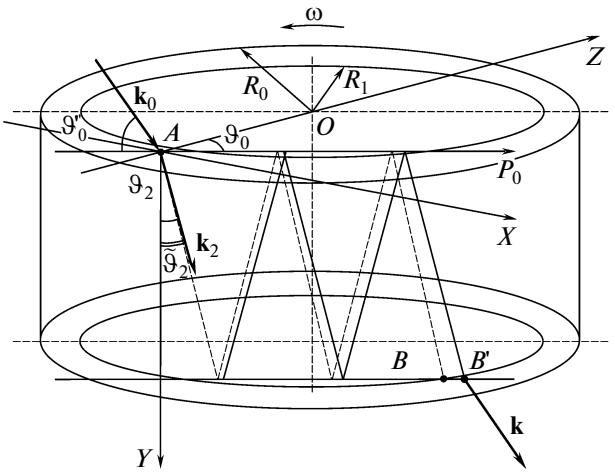

Fig. 1. Reflection coatings (radius R_1) are applied on the flat surfaces of the optical disk (radius R_0) to increase the optical path length in a moving medium. Wavevector $\mathbf{k}_0$ is incident on the optical disk at gliding angle ϑ_0'. If the optical disk is quiescent, the refraction angle is ϑ_2; otherwise (say, counterclockwise rotation), the refraction angle becomes $\tilde{\vartheta}_2$.

In the case in hand, the interferometer has a rotating optical disk inside, which means that the normal projection of the interface velocity is absent. However, there exist a tangential discontinuity of the interface velocity on each flat surface of the disk and the spatial distribution of the velocity field along the wavevector trajectory. This leads to integral expressions for the wavevector trajectory, beam path difference, etc., because of the light beam trajectory distortion [6].

Detailed theoretical description of the interferometer implies consistent application of the coordinate solution to the dispersion relation at each interface and boundary conditions. The boundary conditions consist of (i) the condition of equality of the electromagnetic wave frequencies on both sides of the velocity discontinuity in the frame of reference where the system is quiescent and (ii) the condition of equality of the wavevector tangential components at each interface. A theoretical model must also include kinematic equations for the time coordinates of intersections between light beams and moving interfaces with allowance for dispersion in the medium and may include equations for the interfering beam amplitudes. Such a model may be efficient when the interferometer is described in an inertial frame of reference, in which the instrument as a whole and some of its parts move with different velocities, and also when the interferometer is in a quasi-inertial reference system. Specifically, ring interferometers installed on the earth are expected to exhibit the Sagnac effect because of daily rotation. Testing the model for the invariance of the fringe position is an independent problem of interest.

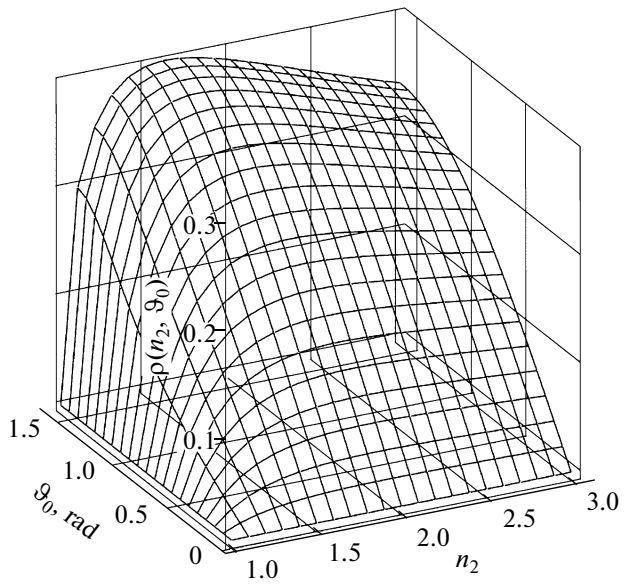

Fig. 2. Transverse light entrainment efficiency vs. refractive index n_2 and angle of incidence ϑ_0.

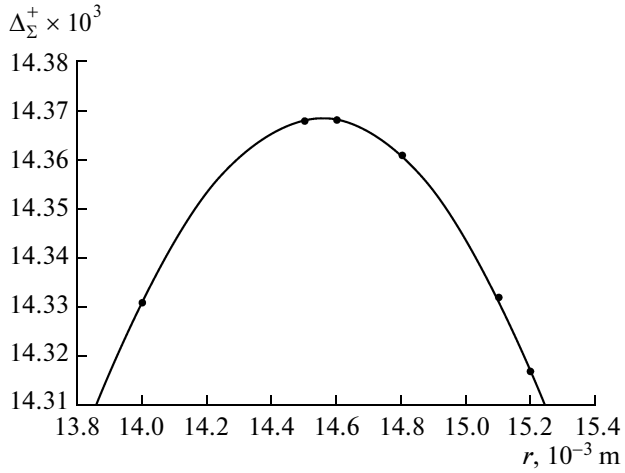

Fig. 3. Total path length difference Δ_Σ^+ vs. parameter r.

In this work, a ring interferometer with a rotating optical disk, which is used to calculate the fringe shift due to light entrainment by a rotating medium under laboratory conditions and compare model results with experimental data, is described using only some elements of the general theoretical model.

In the scheme depicted in Fig. 1, beams are introduced and extracted through the flat surfaces of the disk; therefore, the longitudinal and transverse entrainments of light waves make a major contribution to the phase incursion. The contributions of these effects can be calculated independently owing to the superposition principle.

The path difference of beams propagating through an optical disk in opposite directions and experiencing longitudinal entrainment is given by [18]

$$\Delta_0 = \frac{2l}{\lambda}\frac{\beta_{2n}(n_2^2-1)}{1-n_2^2\beta_{2n}^2}. \quad (2)$$

Here, $\beta_{2n} = \pm V_{2n}/c$, $V_{2n} = 2\pi\nu r$ is the velocity of the optical disk projected onto AP, $l = AB' = 2\sqrt{R^2-r^2}$, n_2 is the refractive index of the optical disk in the frame of reference where the optical disk is quiescent, and $\lambda = 2\pi/k_0$. From expression (2) it follows that Δ_0 reaches a maximum at $r = r_0 = R/\sqrt{2}$.

Since escape point B of the beam shifts from the disk to point B', the transverse entrainment depends on thickness d of the disk and number N of passages of the beam between the flat surfaces of the optical disk,

$$\Delta' = \frac{2Nd(n_2-1)}{\lambda}\left(\frac{1}{\cos\tilde{\vartheta}_2} - \frac{1}{\cos\vartheta_2}\right). \quad (3)$$

For $\tilde{\vartheta}_2$, we have [20]

$$\cos\tilde{\vartheta}_2 = \frac{n_2\cos\vartheta_2 - \kappa_2\beta_{2n}}{\sqrt{n_2^2 - 2n_2\kappa_2\beta_{2n}\cos\vartheta_2 + \kappa_2^2\beta_{2n}^2}}, \quad (4)$$

$$\kappa_2 = n_2^2 - 1.$$

If $\beta_{2n}^2 \ll \beta_{2n}$, expression (3) takes the form

$$\Delta' = \frac{2Nd(n_2-1)\kappa_2\beta_{2n}}{\lambda n_2}\tan^2\vartheta_2. \quad (5)$$

Taking into account that $Nd\tan\vartheta_2 = l$, we can write for the total entrainment of light

$$\Delta_\Sigma^\pm = \Delta_0 \pm \Delta' = (1 \pm \rho(n_2, \vartheta_0))\Delta_0 = \sigma^\pm\nu, \quad (6)$$

where

$$\sigma^\pm = (1 \pm \rho(n_2, \vartheta_0))\frac{4\pi lr(n_2^2-1)}{\lambda c},$$
$$\rho(n_2, \vartheta_0) = \frac{n_2-1}{n_2}\tan\vartheta_2 = \frac{n_2-1}{n_2}\frac{\sin^2\vartheta_0}{\sqrt{n_2^2-\sin^2\vartheta_0}}. \quad (7)$$

Here, function $\rho(n_2\ \vartheta_0)$ characterizes the transverse entrainment efficiency. Its sign depends on the beam path length in the interferometer. Solution (7) is presented in Fig. 2. Let us find the maximal value of ρ, ρ^m. We take into consideration that $\tan\vartheta_2$ is limited from above by angle of incidence $\vartheta_0 \longrightarrow 90°$. In this limit, we have

$$\rho(n_2) = \frac{1}{n}\sqrt{\frac{n_{2-1}}{n_2+1}}. \quad (8)$$

This function has a maximum at $n_2 = (1+\sqrt{5})/2 = 1.618034$. Substituting this value into (8) yields

$$\rho^m = \frac{\sqrt{2(\sqrt{5}-1)}}{3+\sqrt{5}} = 0.3.$$

The presence of the maximum is explained by competition between two effects: as n_2 grows, on the one hand, the optical path increases but on the other hand, ϑ_2, and hence, the geometrical path, decreases.

Let us now find an optimal relationship between r and R with regard to the transverse entrainment for the case when the longitudinal and transverse entrainments are summed up. For Δ_Σ, we can write

$$\Delta_\Sigma = (1 + \alpha\sqrt{R^2 - r^2})\beta r\sqrt{R^2 - r^2}, \quad (9)$$

where ν is the rotation frequency of the optical disk,

$$\alpha = \frac{2}{(Nd)}\frac{n_2 - 1}{n_2}, \quad \beta = \frac{8\pi(n_2^2 - 1)\nu}{\lambda c}.$$

Let us now find the value of r maximizing Δ_Σ. A numerical solution to (9) for $R = 21.5$ mm, $d = 0.02$ m, $N = 3$, $n_2 = 1.71250$ (TF3 optical glass), $\nu = 200$ Hz, and $\lambda = 0.6328$ μm is presented in Fig. 3.

It follows from Fig. 3 that Δ_Σ is maximal at $r = 14.6$ mm instead of $r_0 = R/\sqrt{2} = 15.2$ mm.

Thus, we can conclude that the amount of the transverse entrainment may reach 30% of that of the longitudinal entrainment, which is characterized by quantity Δ_0 in the scheme shown in Fig. 1. With this in mind, the introduction of beams into a moving optical medium should be optimized. The net effect depends on the beam trajectory between the moving optical medium and the plane of the interference pattern.

INTERFEROMETER AND ESTIMATION OF THE EXPECTED EFFECT

Experiments are conducted on a dual-beam interferometer with a rotating optical disk the flat surfaces of which are covered by mirror coatings. Light propagates through the disk in opposite directions (Fig. 4). The ring scheme of the interferometer with an optical disk is very stable and noise immune.

In the interferometer, a beam from stabilized laser L passes through optical scheme $OS1$ and is divided into two beams by beam splitter $BS2$. These two beams, having reflected from mirrors $M1$ and $M2$, pass through the rotating optical disk in opposite directions. Because of rotation, one beam acquires a positive phase shift and the other acquires a negative one. After the beams have met each other again on $BS2$ and are reflected from mirror $M3$, they pass through optical scheme $OS2$ and are detected by photodetector $PD2$. Beam splitter $BS1$ and photodetector $PD1$ are needed to control the laser output.

A helium–neon laser with vertical polarization operating at wavelength $\lambda = 0.632991$ μm is applied. The diameter of the optical disk is $D = 62$ mm, the path length of one beam projected onto the flat surface of the disk is $L = 41$ mm, the refractive index of the glass is $n = 1.71250$ for $\lambda = 632.8$ nm, the thickness of the disk is $d = 10$ mm, and the angle of incidence of the beam on the flat surface of the disk is $\vartheta_0 = 60°$. The rotation frequency of the disk varies from experiment to experiment and may reach $\nu = 250$ Hz.

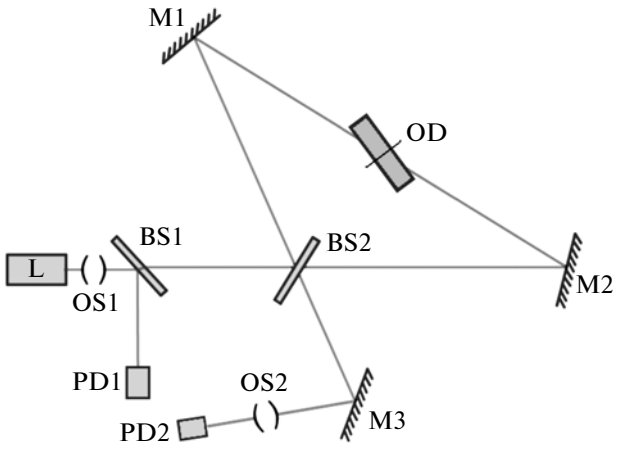

Fig. 4. In the interferometer, a beam from laser L is divided by beam splitter BS2 into two beams propagating through the rotating optical disk in opposite directions. Because of rotation, one beam acquires a positive shift and the other negative.

Let us make estimates for $r = 20.5$ mm.

If the transverse entrainment of light makes an additional contribution to the shift of the interference pattern, the resulting shift is $\Delta_\Sigma^+ = 0.031–0.043$ fringes.

If the transverse entrainment of light shifts the interference pattern to the opposite direction (compared with the longitudinal entrainment), the resulting shift is $\Delta_\Sigma^- = 0.017–0.024$ fringes. The shift is determined by the scheme of the interferometer.

The interferometer rests on two optical platforms with a passive vibration damping system. One of the platforms bears an electrical motor with the optical disk; the other, the rest of the interferometer. Both platforms are mounted on a rotating support allowing the interferometer to rotate through an angle of 360° in the forward and backward directions. Rotation is accomplished with a step motor. The rotating system was aimed, first, at finding the most noise-proof position, at which external noise, such as the vibration of the support, has the least influence and, second, at estimating possible angular and time variations of the interference pattern position.

The interferometer was placed in a chamber with an active system of temperature control. The temperature stabilization accuracy was 0.1°C. The temperature inside and outside the chamber, as well as the rotation angle, was recorded by a photoelectron system and then processed in a PC.

The light was rereflected from the flat surfaces of the optical disk. The reflection interference coatings

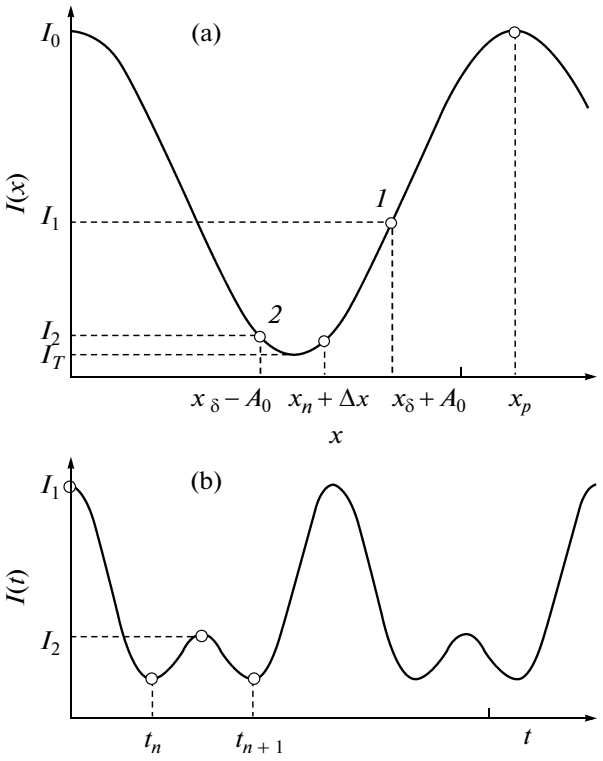

Fig. 5. (a) Coordinate dependence of fringe intensity $I(x)$ and (b) the time dependence of fringe intensity $I(t)$ on the photodetector.

on the flat surfaces of the disk were intended for the laser wavelength.

The shift of the interference pattern was determined from the change in the fringe time consecution on the aperture of the photodetector. The measuring technique is described elsewhere [17, 20]. Since the interferometer is tuned to the same working point in the phase curve throughout all measurement procedures, the shift of the interference pattern is proportional to the fringe time consecution in a first approximation.

Initially, signals were processed with National Instruments PCI-6024 ADCs at an input resolution of 12 bits per channel and PCI-6132 ADCs with a digitization rate of 2.5 MHz and an input resolution of 14 bits per channel. Signals from the measuring photodetector and the photodetector controlling the laser output and sensors measuring the temperature inside and outside the interferometer were applied to the input of the ADCs. Digitized signals were applied to the PC and were further processed in the LabVIEW environment.

Before measurements, the interferometer was tuned so that one, two, or three fringes per revolution of the optical disk will pass in the horizontal direction on the photodiode aperture: in one direction in the first half of the period and in the opposite direction in the other half of the period. The measurand here is Δt: the time interval for which a given fringe travels the photodiode aperture. Since this quantity depends on rotation period T of the optical disk, it was normalized to T.

CALIBRATION OF THE INTERFEROMETER

Calibration of the interferometer consists in finding a relationship between the fringe shift and time signal picked up from the photodetector with fringes periodically traveling over its aperture.

Consider equithickness fringes. Let the interferometer be tuned so that the center of the photodetector in the plane of the interference pattern has coordinate x_n (Fig. 5a). Fringes shift relative to this position to the right and to the left with amplitude A_0 and frequency ω.

The intensity distribution in plane *PD*2 has the form (Fig. 5a)

$$I(x) = \frac{1}{2}[I_0 + I_T + (I_0 - I_T)\cos(\Omega x + \delta)], \qquad (10)$$

where I_0 and I_T are, respectively, the maximal and minimal intensities of fringes; $\Omega = 2\pi/x_p$ is their spatial frequency; x_p is the fringe width; $\delta = \Omega\Delta x = 2\pi\Delta x/x_p$ is the relative shift (in radians) of the interference pattern due to the light entrainment effect; and Δx is the absolute shift of the interference pattern.

The shift of the interference pattern due to the longitudinal Fizeau effect is given by

$$\Delta_0 = \frac{\Delta x}{x_p}. \qquad (11)$$

The time variation of the signal from the compact fast-response photodetector in plane *PD*2 has the same form as the time dependence of the intensity on the aperture of photodetector *PD*2 (Fig. 5b),

$$U(t) = \frac{1}{2}[U_0 + U_T + (U_0 - U_T) \times \cos(\Omega(x_n + A_0\cos(\omega t) + \delta))]. \qquad (12)$$

Here, U_0 and U_T are the voltages on photodetector *PD*2 corresponding, respectively, to the maximal and minimal intensities of the fringes and x_n is the position to which the interferometer is tuned.

Interval $\Delta t = t_{n+1} - t_n$ between neighboring minima generates a valid signal, the intensity of which depends on the rotation rate of the optical disk and Δx.

The coordinates of the minima of the signal in dark fringes (Fig. 5b) are found from the equation $dI/dt = 0$,

$$t_n^{\pm} = \frac{1}{\omega}\arccos\left(-\frac{\tilde{x}_n - 1/2 + \Delta\tilde{x}_\Sigma^{\pm}}{\tilde{A}_0}\right),$$
$$t_{n+1}^{\pm} = \frac{1}{\omega}\arccos\left(\frac{\tilde{x}_n - 1/2 + \Delta\tilde{x}_\Sigma^{\pm}}{\tilde{A}_0}\right). \qquad (13)$$

Values of the parameters reached in this work versus those reported in [9]

References	ν, Hz	V_{2n}, m/s	l, m	n_2	κ_2	$\kappa_2 V_{2n} l$, m^2/s
[9]	<60	<4.87	0.0072	1.457	1.124	<0.04
This work (new interferometer)	250	32.2	0.041	1.7125	1.9327	3.57

Here, $\tilde{A}_0 = A_0/x_p$, $\tilde{x}_n = x_n/x_p$, and $\Delta\tilde{x}_\Sigma^\pm = \Delta x_\Sigma^\pm/x_p$ and the sign indicates clockwise or counterclockwise rotation.

The width of the interval $\Delta t^\pm = t_{n+1}^\pm - t_n^\pm$ depends on the rotation period of the optical disk; therefore, we normalize its value to rotation period T,

$$\frac{\Delta t^\pm}{T} = \frac{1}{\pi}\arcsin\left(\frac{\tilde{x}_n - 1/2 + \Delta\tilde{x}_\Sigma^\pm}{\tilde{A}_0}\right). \quad (14)$$

Note that the spatial and time shifts of the fringes are related nonlinearly.

Let us find the differential of this expression with respect to $\tilde{\Delta}_\Sigma^\pm$,

$$d\left(\frac{\Delta t^\pm}{T}\right) = \frac{1}{\pi}\frac{2d\tilde{\Delta}_\Sigma^\pm}{\sqrt{4\tilde{A}_0^2 - (2x_n - 1 + 2\Delta\tilde{x}_\Sigma^\pm)^2}}. \quad (15)$$

This expression determines the sensitivity of the interferometer to the fringe shift. Remarkably, rotation frequency ω of the optical disk in this expression is lacking. This is because the spatial shift of fringes and their time shift normalized to the period linearly depend on the rotation frequency, differentials $d\tilde{\Delta}_\Sigma^\pm$ and $d\Delta t^\pm/T$ tend to zero when the rotation frequency tends to zero.

When the fringes shift by $d\tilde{\Delta}_\Sigma^\pm$, the variation of time signal $d\Delta t/T$ reaches a maximum if

$$\tilde{A}_0 = \tilde{x}_n - \frac{1}{2} + \Delta\tilde{x}_\Sigma. \quad (16)$$

Let us introduce the designation $4\tilde{A}_0^2 - (2\tilde{x}_\delta - 1 + 2\tilde{\Delta}_\Sigma^\pm)^2 = \tilde{d}^2$.

Assume that $|\tilde{d}|$ is small (this is easy to realize); then, the relative shift of fringes is estimated as

$$d\tilde{\Delta}_\Sigma^\pm = \frac{\pi\tilde{d}}{2}d\left(\frac{\Delta t^\pm}{T}\right). \quad (17)$$

Now suppose that the minimal detectable fringe-shift-induced signal exceeds the noise level in measuring time interval Δt. Let this level be known from the experiment and the ratio of this level to the rotation period, $d(\Delta t/T)$, be equal to 10^{-4} and let the interferometer be tuned to $\tilde{d} = 0.1$. Then, the limit value of the minimal detectable signal is no lower than $d\Delta = 3 \times 10^{-5}$ of the fringe.

PRELIMINARY RESULTS

The table gives the parameters of our experiment and compares them with those reached in [9]. Here, V_{2n} is the projection of the linear velocity of the optical disk onto the beam, l is the length of the projection of the beam in the optical disk onto its flat surface, n_2 is the refractive index of the optical disk, and $\kappa_2 = n_2^2 - 1$. Since the light entrainment depends on the product $(n_2^2 - 1)V_{2n}l$ in the zeroth approximation, entrainment efficiency $\kappa_2 V_{2n} l$ is given in the last column.

The typical spectrum of the initial interference signal picked up from detector PD2 is shown in Fig. 6. The major peak is observed at the rotation frequency of the optical disk (about 200 Hz).

The interference signal was processed as follows. First, extreme points in signal $I(t)$ were found by the least-squares method. Then, the interval $\Delta t = t_{n+1} - t_n$ was calculated.

To find an optimal relationship between A_0 and x_δ, we express $\tilde{A}_0$ as

$$\tilde{A}_0 = \sqrt{\tilde{d}^2/4 + \delta_x^2}. \quad (18)$$

Here, $\delta_x = \tilde{x}_\delta - 1/2$ is the detuning parameter characterizing the shift of the working point from the dark fringe. The δ_x dependence of $\tilde{A}_0 - \delta_x$ for $\tilde{d} = (0.05, 0.10, 0.20)$ is shown in Fig. 7 in the range $\delta_x = 0$–0.2.

The difference $\tilde{A}_0 - \tilde{x}_\delta$ falls rapidly, which means that the secondary peak in the signal diminishes and the signal will be difficult to separate. It is desirable to

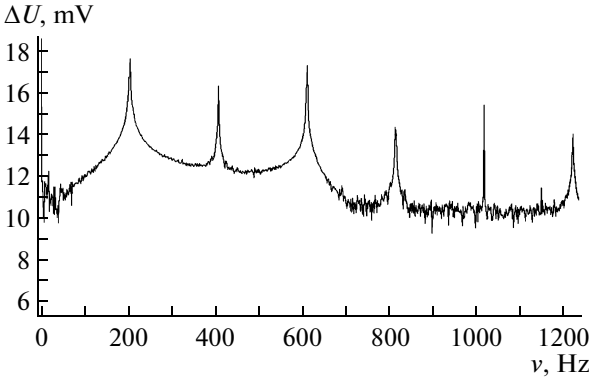

Fig. 6. Spectrum of the initial interference signal.

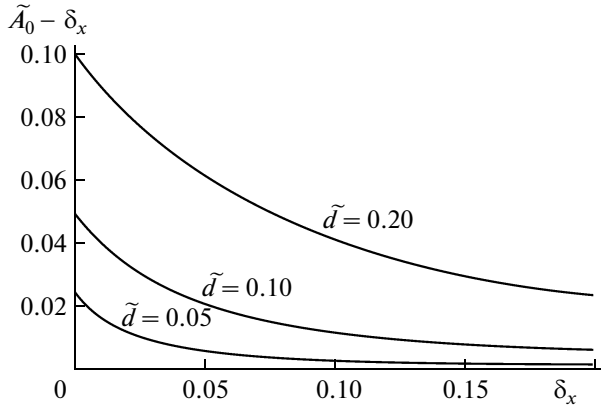

Fig. 7. δ_x dependence of the difference $\tilde{A}_0 - \delta_x$ for different values of d.

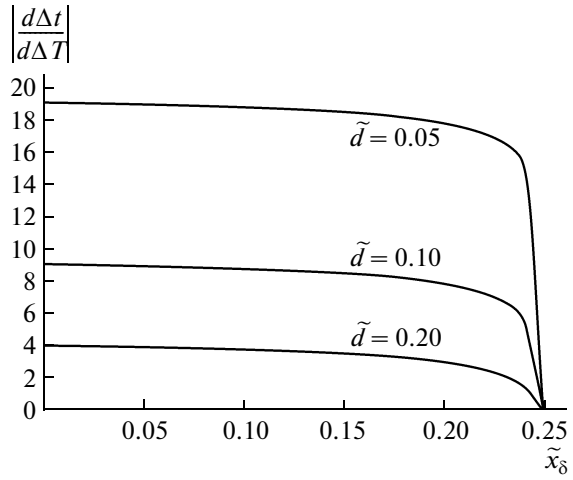

Fig. 8. $|d\Delta t/d\Delta T|$ vs. $\tilde{x}_\delta$ for different values of d.

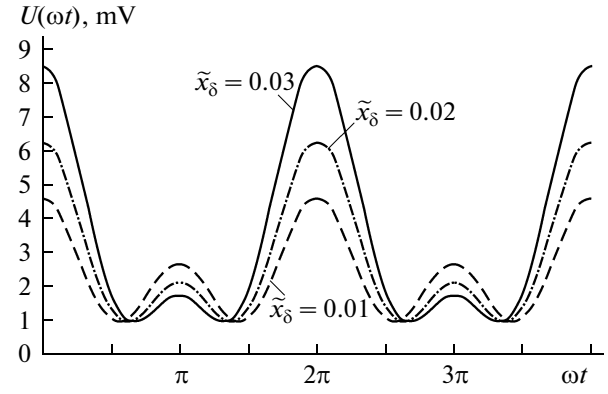

Fig. 9. Theoretical dependence of voltage $U(\omega t)$ applied to the photodetector on ωt for different values of $\tilde{x}_\delta$.

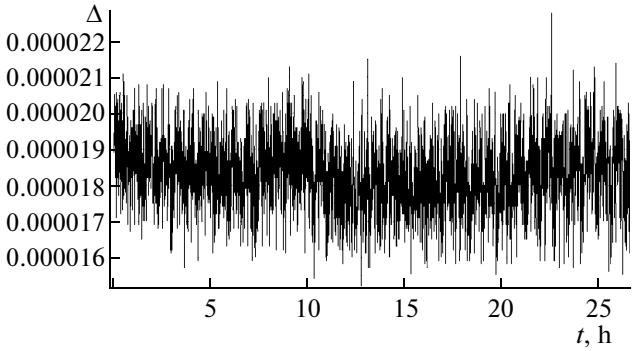

Fig. 10. Estimated absolute error of $\Delta t/T$ determination as a function of time.

take the largest value of the difference for a given value of parameter $\tilde{d}$. Figure 8 plots the $\tilde{x}_\delta$ dependence of $|(d/d\Delta)(\Delta t/T)|$.

It is seen that ratio $|(d/d\Delta)(\Delta t/T)|$ depends on $\tilde{x}_\delta$ only slightly, which simplifies tuning.

Let the voltage on the *PD*2 detector be described by function (12).

We put $(U_0 + U_t)/2 = 51$ mV, $(U_0 - U_T)/2 = 50$ mV, $\delta = 0$, and $\tilde{d} = 0.1$. For $d = 0.1$, we select $\tilde{x}_\delta = x_\delta/x_p = 0.02$ and find that $A_0 = 0.0539$. Thus, taking different $\tilde{x}_\delta$, one can obtain different shapes of variable signal $U(\omega t)$. Figure 9 shows the shapes of the signal at $\tilde{x}_\delta = (0.01, 0.02, 0.03)$.

At smaller $\tilde{x}_\delta$, the secondary maximum becomes more pronounced and the signal processing quality improves.

The fringe width can be found from (12),

$$x_p = \frac{1}{2\pi(x_\delta + A_0\cos\omega t)}\arccos\frac{2U(t) - U_0 - U_T}{U_0 - U_T}. \quad (19)$$

At the first stage of the experiment, we recorded the signal for a long time (24–25 h) with the supply voltage of the optical-disk-driving motor fixed. The rotation frequency in this case remained constant up to 0.5 Hz. Having processed a daily data array, we found that the signal mean deviation is at a level of 10^{-3} and the accumulated error is 2 s, that is, on the order of 2×10^{-5} at limited statistical processing.

The time variation of the absolute error of Δt measurement is presented in Fig. 10.

Thus, the signal-to-noise ratio is on the order of 10^{-4} throughout a day, which confirms the high stability of measurements.

Assuming that the noise level in our experiments was $d(\Delta t/T) = (1–7) \times 10^{-4}$, we can conclude that in the best experiment with $d(\Delta t/T) = 10^{-4}$ and tuning

$\tilde{d} = 0.1$, fringe shift $d\Delta = 3 \times 10^{-5}$ could be detected. Analysis shows that time variations $\delta\Delta$ of the daily record does not exceed this value. On the one hand, this value can be viewed as an accuracy estimate; on the other hand, it may serve as an upper bound of possible laboratory space anisotropy.

At the second stage of the experiment, the rotation frequency of the optical disk was varied. Initially, the signal was recorded for 1 min with the supply voltage of the optical-disk-driving motor fixed; then, the supply voltage of the motor was changed by 0.2 V and, after the transient, the signal was recorded again, etc. The range of the rotation frequency is related to a small change in the shape of the time-dependent signal and to the need to change the aperture of the filter. This makes an additional contribution to the signal and distorts the dependence of the fringe shift on the velocity of the medium. This problem was solved by processing the signal with a method based on well-known analytical formula (12) for the time-dependent signal. The signal parameters were restored using the Jacobi–Anger expansion.

In this work, we experimentally determined the dependence of ratio $\Delta t/T$ (where Δt is the time the fringe takes to travel the photodiode aperture and T is the rotation period) on rotation frequency ν of the optical disk for rotation in both directions. That this dependence is nonlinear follows from expression (14) and is corroborated by calculations. Figure 11 demonstrates the result of conversion of the dependence of $\Delta t/T$ on rotation frequency ν to the dependence of spatial shift Δ_Σ on the rotation frequency of the optical disk for both senses of rotation. The slopes of the straight lines differ but are of the same sign, which means that elastic strain makes the same contribution irrespective of the sense of rotation.

The difference between the values of $\Delta_\Sigma(\nu)$ and $\Delta_\Sigma(-\nu)$ obtained for forward and backward rotations, respectively, at each frequency indicated in the curves represents an experimental dependence of the doubled amount of the light entrainment effect on the rotation frequency of the optical disk.

Theoretical estimation gives $\Delta_\Sigma = 1.34 \times 10^{-4}\nu$. We also obtained an experimental dependence of Δ_Σ on rotation frequency ν of the optical disk, $\Delta_\Sigma^{\text{exp}} = 1.2 \times 10^{-4}\nu$, which is in agreement with the statements of contemporary electrodynamics of moving media. A difference of 10% between the proportionality factors may be explained by the incorrect adjustment of the interferometer to the calculated value of r. In addition, the difference between the observed and calculated amounts of the light entrainment effect can be explained by the feature of signal filtering. The signal was recorded at a fixed discretization rate of the ADC; therefore, the number of points per period of the signal varies with the rotation frequency of the optical disk, causing a systematic error.

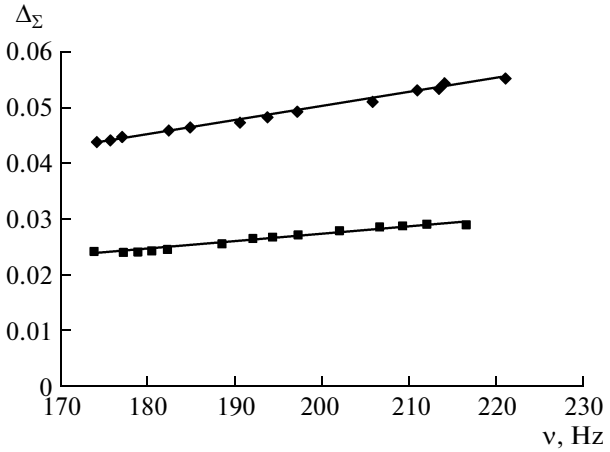

Fig. 11. Fringe shift Δ_Σ measured over aperture of the photodetector as a function of rotation frequency ν for forward and backward rotations.

The signal-to noise ratio in the given measuring technique can be increased further by using multielement photodetectors and eliminating the influence of the elastic deformation of vibration-damping elements.

CONCLUSIONS

An optical scheme and an interferometer built on their basis are suggested for investigating effects inherent in the optics of moving media. They offer difference compensating properties and allow high-precision studies of the electromagnetic wave propagation in a rotating optically transparent medium to be performed.

Our experiments confirm the linear dependence of the fringe shift on the velocity of the medium up to 29.5 m/s.

The time variation of the fringe position at a fixed rotation velocity of the optical disk was recorded accurate to 3×10^{-5} fringes.

The optical scheme and method of fringe shift measurement embody ways of improving the sensitivity and noise immunity, such as the use of detector arrays, stabilization of the optical disk rotation frequency, suppression of the dynamic elastic deformation of vibration-damping elements, and the use of a refined signal processing technique based on the well-known analytical shape of the time-dependent signal.

Note also that the dependences presented in Fig. 11 were obtained without using multibeam schemes for accumulating the phase difference between interfering beams. That is, even if the velocity of the medium is nonrelativistic and the electromagnetic wave passes through the medium only once, it contains information on the velocity of the medium, which can be measured with a sufficient accuracy. This provides the basis

for developing new contactless techniques for measuring the kinematic parameters of motion.

Calculations show that the theoretical apparatus of the optics of moving media can and must be applied in laser location, coherent data transfer between orbiting vehicles and earth stations, space navigation, numerical simulation of interferometers intended for detection of gravitational waves, and in other problems where electromagnetic radiation interacts with a moving medium. Finally, it should be employed to describe the propagation of electromagnetic radiation in the atmospheres of astrophysical objects and a moving intergalactic medium on a cosmological scale.

REFERENCES

1. B. M. Bolotovskii and S. N. Stolyarov, Sov. Phys. Usp. **32**, 813 (1989).
2. G. Sagnac, C. R. Acad. Sci. **33**, 349 (1913).
3. H. d'Fizeau, Ann. Chim. Phys. **57**, 385 (1859).
4. E. J. Post, Rev. Mod. Phys. **39**, 475 (1967).
5. H. J. Arditty and H. C. Lefevre, Opt. Lett. **6** (8), 401 (1981).
6. V. O. Gladyshev, JETP Lett. **58**, 569 (1993).
7. A. A. Logunov and Yu. V. Chugreev, Sov. Phys. Usp. **31**, 861 (1988).
8. C. V. Heer, Phys. Rev. A **134**, 799 (1964).
9. H. R. Bilger and W. K. Stowell, Phys. Rev. A **16**, 313 (1977).
10. W. R. Leeb, G. Schiffner, and E. Scheiterer, Appl. Opt. **18**, 1293 (1979).
11. I. Lerche, Am. J. Phys. **45**, 1154 (1977).
12. V. Vali, R. W. Shorthill, and M. F. Berg, Appl. Opt. **16**, 2605 (1977).
13. O. G. Zagorodnov, Ya. B. Fainberg, and A. M. Egorov, Sov. Phys. JETP **11**, 4 (1960).
14. V. O. Gladyshev, Tech. Phys. **44**, 566 (1999).
15. V. P. Vasil'ev, V. A. Grishmanovskii, L. F. Pliev, and T. P. Startsev, JETP Lett. **55**, 316 (1992).
16. V. P. Vasil'ev, L. I. Gusev, J. J. Dengan, and V. D. Shargorodskii, Radiotekh., No. 4, 80 (1966).
17. V. O. Gladyshev, T. M. Gladysheva, and V. E. Zubarev, Tech. Phys. Lett. **28**, 123 (2002).
18. V. O. Gladyshev, T. M. Gladysheva, M. Dashko, N. Trofimov, and E. A. Sharandin, Tech. Phys. Lett. **33**, 905 (2007).
19. V. O. Gladyshev, T. M. Gladysheva, M. Dashko, N. Trofimov, and E. A. Sharandin, Giperkompleksnye Chisla Geom. Fiz. **3**, 173 (2006).
20. V. Gladyshev, T. Gladysheva, and V. Zubarev, J. Eng. Math. **55** (1–4), 239 (2006).